Supporting Information

f

Xiaoying Lu[a,1], Minmin Cai[a,1], Zehua Zou[a], Junfeng Huang[a], Cailing Xu[a]*

[a] State Key Laboratory of Applied Organic Chemistry, Laboratory of Special Function Materials and Structure Design of the Ministry of Education, College of Chemistry and Chemical Engineering, Lanzhou University, Lanzhou 730000, China

*Email: xucl@lzu.edu.cn

Experiment Section

Materials: Sodium molybdate dehydrate ($NaMoO_4 \cdot 2H_2O$) was obtained from Sinopharm Chemical Reagent Co. Ltd. (Shanghai, China). Nickel nitrate hexahydrate ($Ni(NO_3)_2 \cdot 6H_2O$), nickel chloride hexahydrate ($NiCl_2 \cdot 6H_2O$) and potassium dihydrogen phosphate (KH_2PO_4) were purchased from Xilong Chemical Reagent Co. Ltd. (Chendou, China). Anhydrous ethanol (CH_3CH_2OH), hydrochloric acid (HCl), acetone (CH_3COCH_3) and sodium hydroxide (NaOH) were provided by Tianjin Pharmaceutical Chemical Reagent Co. Ltd. (Tianjin, China). Platinum (20 wt% on carbon black) was purchased from Alfa Aesar. Nickle foam with a thickness of 1.6 mm and a pore density of 110 ppi was purchased from Changsha Keliyuan. All chemicals were used directly without further purification. The deionized water (DI-water) was used throughout the experiment.

Preparation of $NiMoO_4$-$Mo_{0.84}Ni_{0.16}$ composites: Firstly, Ni foam (2 cm×4 cm) was ultrasonically cleaned with 6 M HCl solution, acetone, anhydrous ethanol and DI-water for 10 min, respectively, successively to remove the oxide and oil on the surface

of Ni foam, then dried at room temperature.

Secondly, $NiMoO_4 \cdot xH_2O$ precursors were synthesized on the NF by a facile hydrothermal process. Typically, 1.5 mmol $Ni(NO_3)_2 \cdot 6H_2O$ and 1.5 mmol $NaMoO_4 \cdot 2H_2O$ were dispersed in 35 mL DI water under sustained magnetic stirring to form a clear and green solution. Then, the obtained homogeneous solution and a piece of Ni foam were transferred to a 50 mL Teflon-lined stainless steel autoclave. The autoclave was then sealed and heated at 150 ºC for 6 h. Following this, the autoclave cooled naturally in air. Finally, the obtained Ni foam was taken out, washed several times with with DI water and ethanol, respectively and dried at 60 ˚C.

Finally, the growth of Mo-Ni alloy nanoparticles on the surface of the substrate was performed by direct reduction of $NiMoO_4$ under H_2/Ar (5% H_2) atmosphere and kept at 500 ^oC for 2 h with a heating rate of 2 ºC min^{-1}. After being cooled to room temperature, the obtained samples were named as $NiMoO_4$-$Mo_{0.84}Ni_{0.16}$ composites.

Preparation of $Mo_{0.84}Ni_{0.16}$@$Ni(OH)_2$ heterostructure: $Mo_{0.84}Ni_{0.16}$@$Ni(OH)_2$-X heterostructure samples were obtained by a facile electrodeposition method in a standard three electrode system, where the graphite electrode was used as a counter electrode, the saturated calomel electrode (SCE) and the obtained $NiMoO_4$-$Mo_{0.84}Ni_{0.16}$ composites were utilized as the reference electrode and work electrode, respectively. The $Ni(OH)_2$ nanosheets can be grown on the surfaces of $NiMoO_4$-$Mo_{0.84}Ni_{0.16}$ in 0.1 M $NiCl_2$ solution (25 mL) at -1.0 V (SCE) at room temperature. The mass loading of $Ni(OH)_2$ nanosheets on $NiMoO_4$-$Mo_{0.84}Ni_{0.16}$ can be achieved by controlling deposition time such as 500 s, 1000 s and 1500 s. And the samples with

different mass loading of $Ni(OH)_2$ were denoted as $Mo_{0.84}Ni_{0.16}$@$Ni(OH)_2$-5, $Mo_{0.84}Ni_{0.16}$@$Ni(OH)_2$-10 and $Mo_{0.84}Ni_{0.16}$@$Ni(OH)_2$-15, respectively, according to the reaction time.

Characterizations:

X-Ray diffraction (XRD) patterns of the samples were recorded on a Rigaku D/M ax-2400 diffractometer with Cu Kα irradiation at a scanning rate of 10° min^{-1}. The morphology of the samples was investigated by field emission scanning electron microscopy (FESEM, JEOLJSM-S4800) and transmission electron microscopy (TEM, TecnaiTM G2 F30) with energy dispersive spectroscopy (EDX). The X-ray photoelectron spectroscopy (XPS) spectra of the samples were performed on a PHI-5702 instrument with a Mg-Kα excitation source (1253.6 eV). Binding energies (BE) were determined using the C 1s peak at 284.8 eV as a charge reference. The amount of hydrogen was quantified by a computer-controlled GC-2014C gas chromatograph equipped with a thermal conductivity detector at 353 K with argon as carrier gas.

Electrochemical measurements:

All the electrochemical experiments were implemented on an electrochemical station (Metrohm Autolab, PGSTAT302) with a three-electrode system. The working electrode was the as-synthesized samples with a fixed geometric area of 1 cm×1 cm. The Hg/HgO electrode and the graphite rod served as reference and counter electrodes, respectively. Pt/C electrode was prepared as follows: the catalyst powders (5 mg) was ultrasonically dispersed in 1 mL DI water/ethanol mixture solution (V/V=4:1) and 10 μL Nafion solution (5 wt%) to form a homogeneous ink. Then the mixture was coated

onto a piece of Ni foam (the mass loading is 2 mg•cm^{-2}). The linear sweep voltammograms (LSV) were measured at a scan rate of 2 mV•s^{-1} in 1.0 M KOH solution to evaluate HER activities. The electrochemical impedance spectroscopy (EIS) of the electrodes were measured at -0.1 V versus RHE in the frequency range from 100 kHz to 0.01 Hz with an amplitude of 10 mV. To determine the double-layer capacitance (C_{dl}), a series of CV measurements were made at different scan rates (10, 15, 20, 25 and 30 mV•s^{-1}) in a non-Faradaic region (0.15-0.25 V vs. RHE). The chronoampermetry and LSV are used to evaluate the stability of catalysts. All potential data are given versus reversible hydrogen electrode (RHE) according to the following equation:

$$E_{RHE} = E^{\theta}_{Hg/HgO} + E_{Hg/HgO} + 0.059 \times pH \left(pH = 13.6\right) \qquad \text{(S1)}$$

where E^{θ}(Hg/HgO) is the standard electrode potential of Hg/HgO reference electrode (0.098 V versus RHE at 25 ^{o}C).

All LSV curves reported in this work are corrected for iR loss according to the following formula:

$$E_{compensated} = E_{measured} - iR \qquad \text{(S2)}$$

where $E_{compensated}$ is the compensated potential, $E_{measured}$ is the measured potentials and R is the equivalent series resistance that derived from the EIS.

The mass activity could be calculated according to the follow equation:

$$Mass\ activity = \frac{j}{m} \qquad \text{S3}$$

where j is the current density and m is the mass loading of electrocatalysts. The mass loading of $Mo_{0.84}Ni_{0.16}$@$Ni(OH)_2$-10 and Pt/C are 2.8 mg cm^{-2} and 2.0 mg cm^{-2},

respectively, and the current density at an overpotential of 10 mV was used.

The turnover number (TON) is defined as follows:

$$TON = \frac{n_{H_2}}{n} \qquad \text{S4}$$

where n_{H2} and n are the mole amount of hydrogen and the number of active sites of catalyst, respectively. The amount of hydrogen is 255.8 μmol after 1 h electrolysis at η= 100 mV.

The number of active sites was quantified by cyclic voltammetry (CV) method [1,2] (Fig. S5). Since the difficulty in attributing the observed peaks to a given redox couple, the number of active sites should be proportional to the integrated charge over the CV curve. Assuming one-electron process for both reduction and oxidation, the upper limit of active sites (n) for $Mo_{0.84}Ni_{0.16}$@$Ni(OH)_2$-10 could be calculated according to the follow equation:

$$n = \frac{Q}{2F} \qquad \text{S5}$$

where F and Q are the Faraday constant and the whole charge of CV curve, respectively.

The turnover frequency (TOF) is defined as the number of reactant which can convert to a desired product per catalytic site per unit of time. The following formula was used to calculate TOF:

$$TOF = \frac{1}{2}\frac{I}{nF} \qquad \text{S6}$$

where F and n are the Faraday constant and the number of active sites, respectively; I is the current density of LSV curves.

Supplemental Figures and Tables.

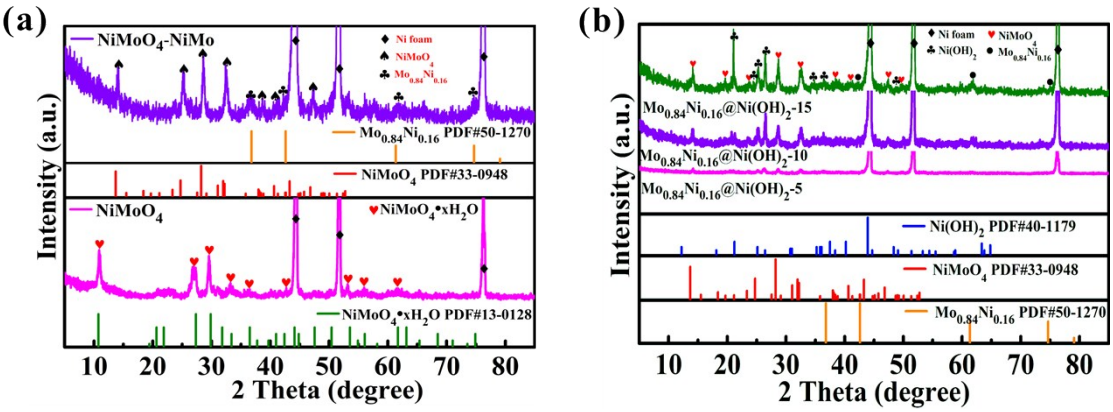

Fig. S1 XRD patterns of (a) $NiMoO_4$ precursors and $NiMoO_4$-$Mo_{0.84}Ni_{0.16}$ composites and (b) $Mo_{0.84}Ni_{0.16}$@$Ni(OH)_2$-5, $Mo_{0.84}Ni_{0.16}$@$Ni(OH)_2$-10 and $Mo_{0.84}Ni_{0.16}$@$Ni(OH)_2$-15.

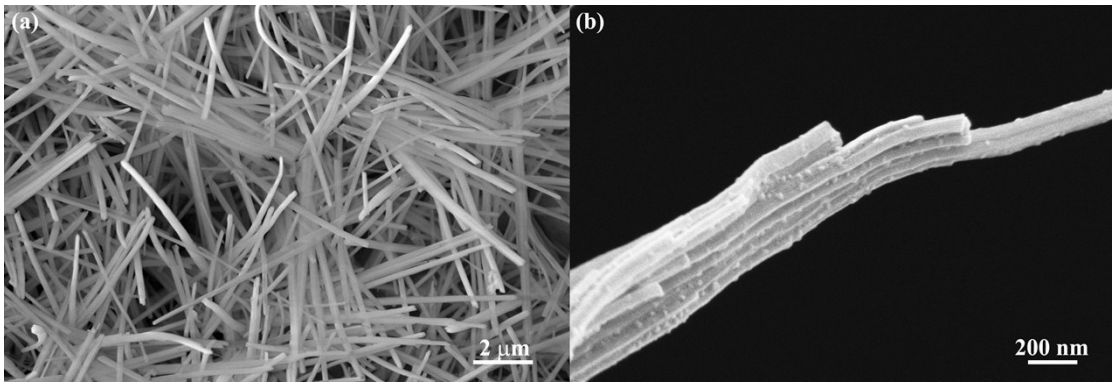

Fig. S2 SEM images of (a) $NiMoO_4$ precursors and (b) $NiMoO_4$-$Mo_{0.84}Ni_{0.16}$ composites.

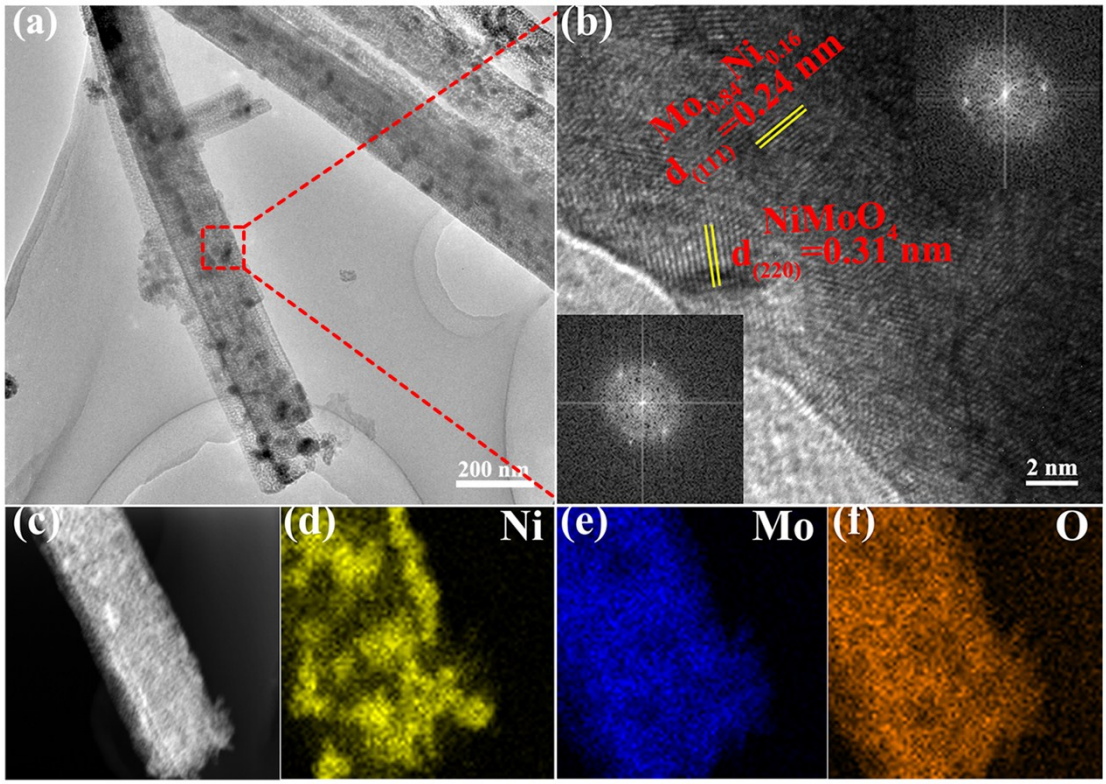

Fig. S3 (a) TEM, (b) HRTEM, (c) STEM and (d-f) the corresponding elemental mapping images of $NiMoO_4$-$Mo_{0.84}Ni_{0.16}$ composites.

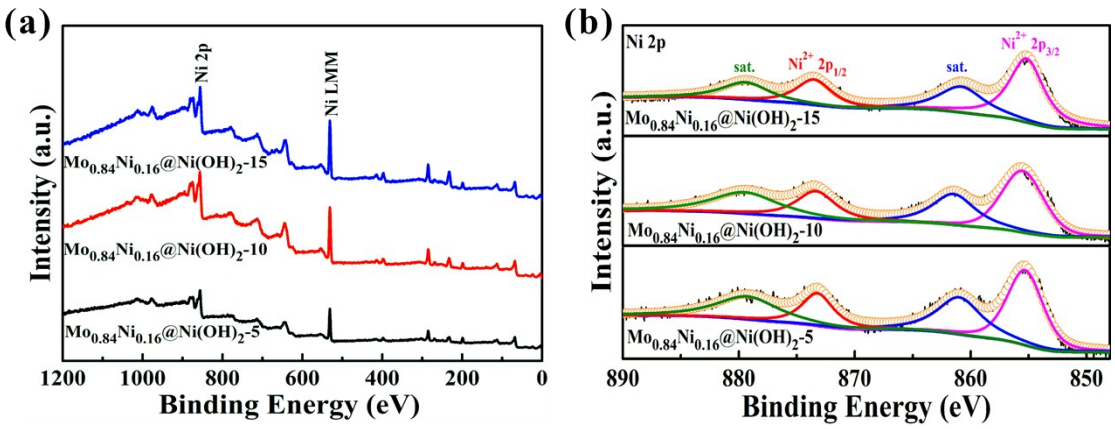

Fig. S4 (a) XPS survey spectra and (b) High resolution XPS spectra of Ni 2p for $Mo_{0.84}Ni_{0.16}$@$Ni(OH)_2$-5, $Mo_{0.84}Ni_{0.16}$@$Ni(OH)_2$-10 and $Mo_{0.84}Ni_{0.16}$@$Ni(OH)_2$-15 heterostructures.

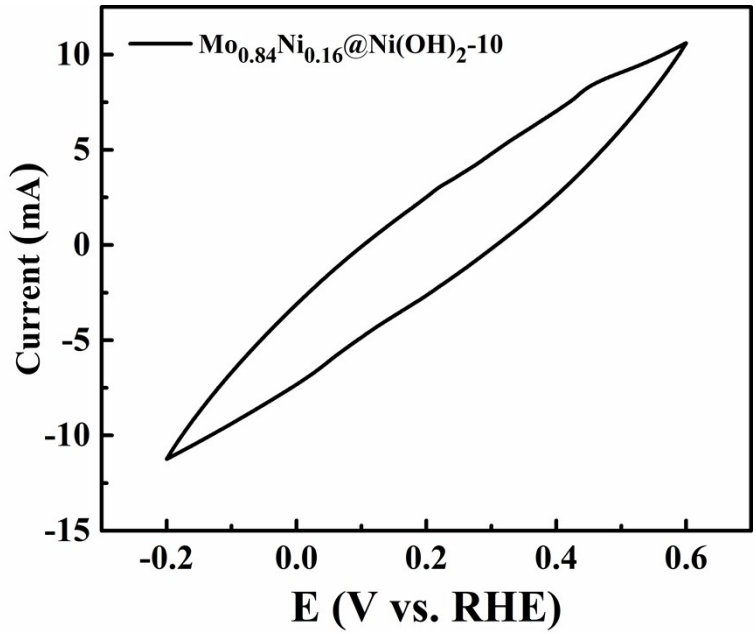

Fig. S5 CV curve of $Mo_{0.84}Ni_{0.16}$@$Ni(OH)_2$-10 recorded between -0.2 V and 0.6 V vs. RHE in 1.0 M PBS (pH=7) at a scan rate of 50 mV s^{-1}.

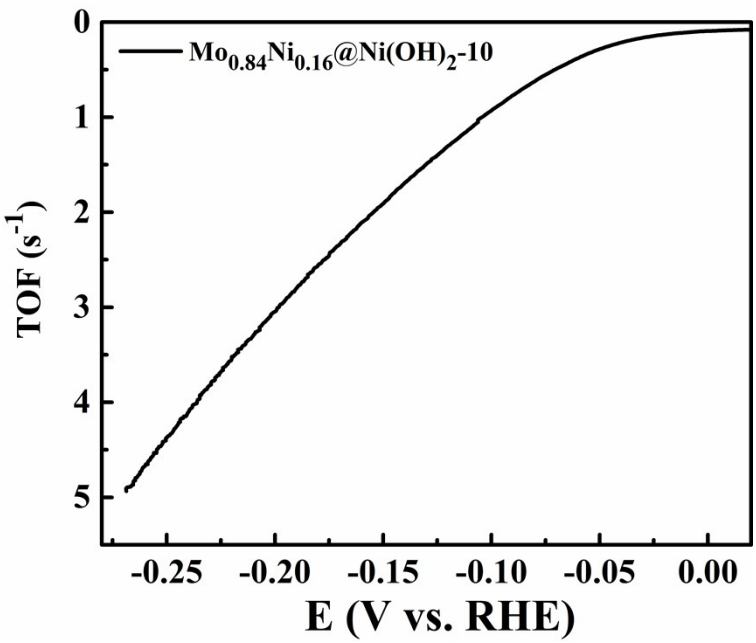

Fig. S6 The calculated TOF of $Mo_{0.84}Ni_{0.16}$@$Ni(OH)_2$-10.

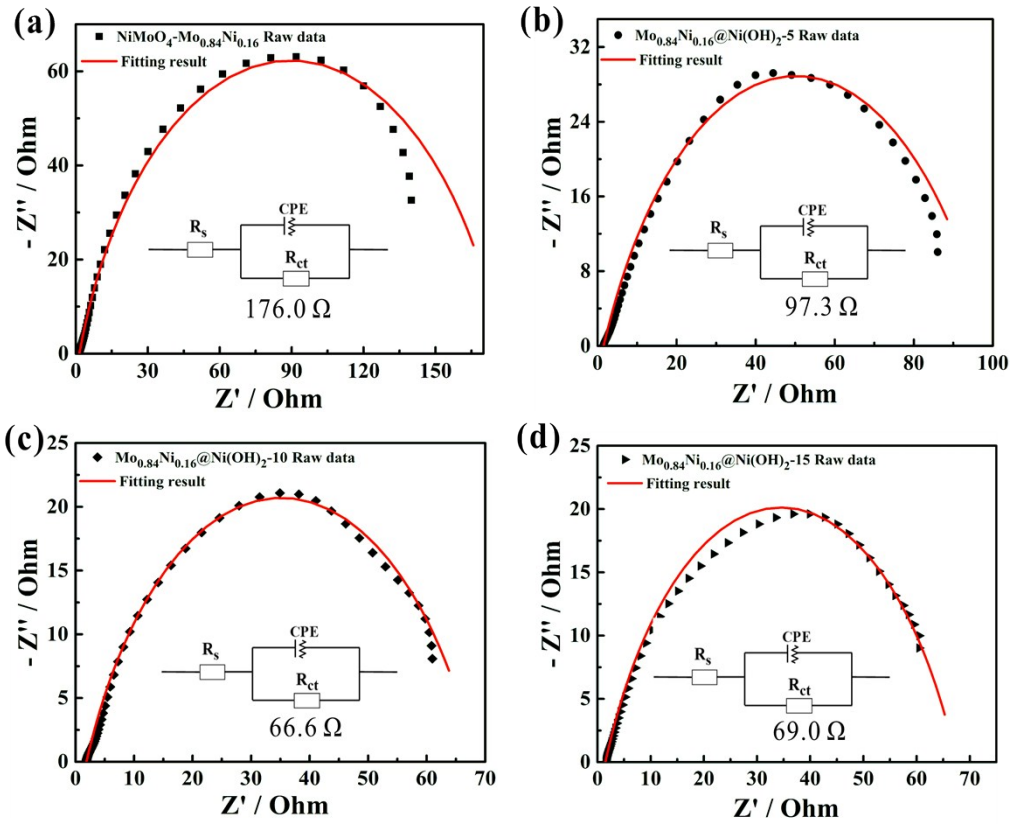

Fig. S7 Electrochemical impedance spectroscopy of (a) $NiMoO_4$-$Mo_{0.84}Ni_{0.16}$, (b) $Mo_{0.84}Ni_{0.16}$@$Ni(OH)_2$-5, (c) $Mo_{0.84}Ni_{0.16}$@$Ni(OH)_2$-10 and (d) $Mo_{0.84}Ni_{0.16}$@$Ni(OH)_2$-15. The inset is the equivalent circuit used for fitting.

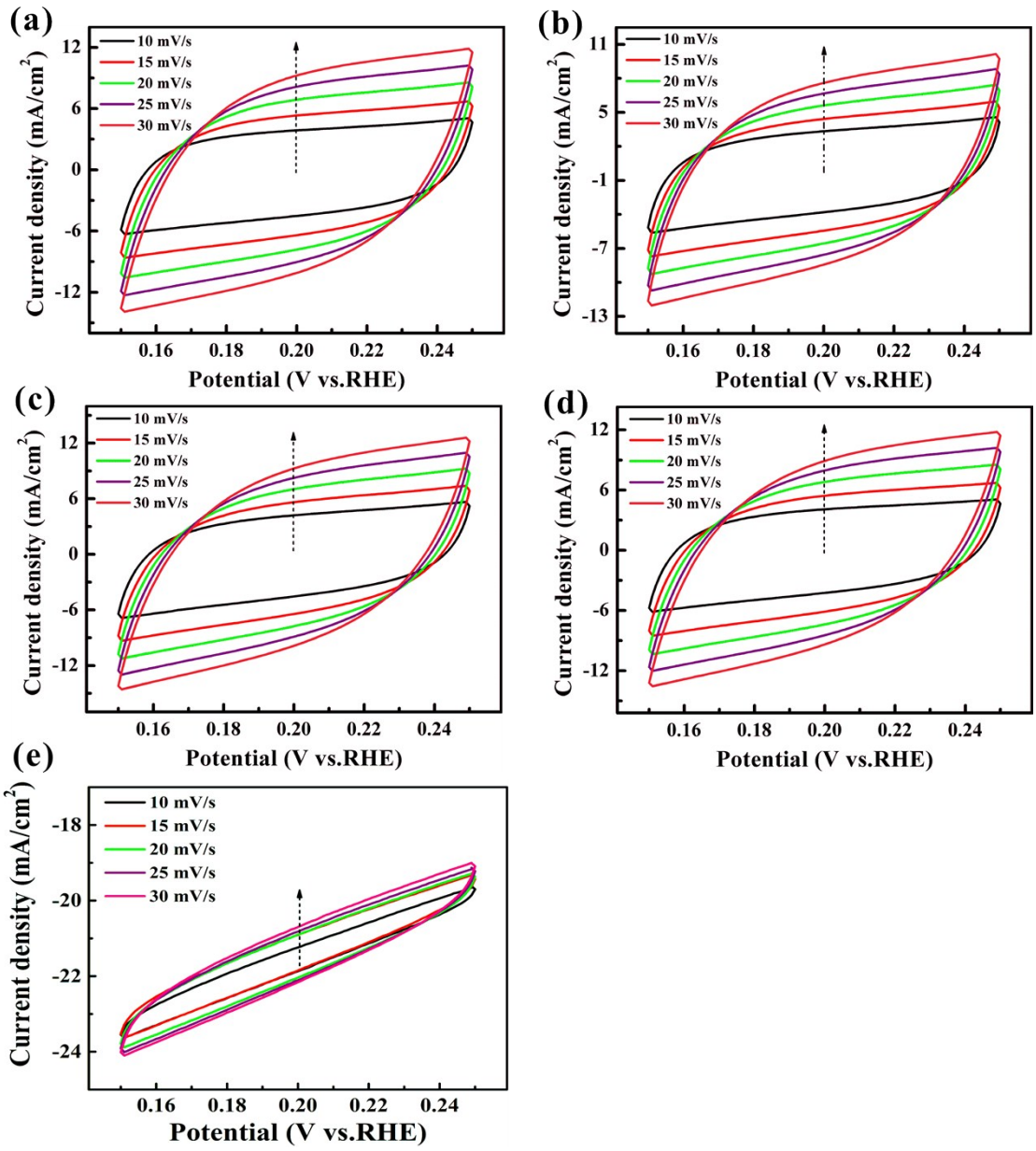

Fig. S8 CV curves at different scan rates between 0.15 and 0.25 V vs. RHE for (a) $NiMoO_4$-$Mo_{0.84}Ni_{0.16}$, (b) $Mo_{0.84}Ni_{0.16}$@$Ni(OH)_2$-5, (c) $Mo_{0.84}Ni_{0.16}$@$Ni(OH)_2$-10, (d) $Mo_{0.84}Ni_{0.16}$@$Ni(OH)_2$-15 and (e) Pt/C.

Table S1 Overpotential and Tafel slope of the reported noble-free electrocatalysts.

Catalysts	Electrolyte	η_{10} (mV)	Tafel Slope (mV/dec)	Reference
Ni-MoS_2	1 M KOH	98	60	3
MoS_2-C	1 M KOH	149	82	4
MoS_2-Ni_3S_2 HNRs/NF	1 M KOH	98	61	5
Cu NDs/Ni_3S_2 NTs-CFs	1 M KOH	128	76	6
MoP/CNT	1 M KOH	86	73	7
Ni_3N/Ni	1 M KOH	12	80	8
V-Co_4N	1 M KOH	37	44	9
$MoNi_4/MoO_{3-x}$	1 M KOH	17	36	10
Ni NP|Ni–N–C	1 M KOH	147	114	11
MoP@PC	1 M KOH	97	59.3	12
MoNi/$CoMoO_3$/NF	1 M KOH	18	35	13
$V_2O_5/Ni(OH)_2$	1 M KOH	39	44	14
$Mo_{0.84}Ni_{0.16}$@$Ni(OH)_2$	1 M KOH	10	71	This work

Reference:

1. D. W. Wang, C. Han, Z. C. Xing, Q. Li, X. R. Yang, J. Mater. Chem. A, 2018, 6, 15558-15563.

2. Y. Y. Chen, Y. Zhang, X. Zhang, T. Tang, H. Luo, S. Niu, Z. H. Dai, L. J. Wan, J. S. Hu, Adv. Mater., 2017, 29, 1703311.

3. J. Zhang, T. Wang, P. Liu, S. H. Liu, R. H. Dong, X. D. Zhuang, M. W. Chen and X. L. Feng, Energy Environ. Sci., 2016, 9, 2789-2793.

4. Z. X. Wu, J. Wang, R. Liu, K. D. Xia, C. J. Xuan, J. P. Guo, W. Lei, D. L. Wang, Nano Energy, 2017, 32, 511-519.

5. Y. Q. Yang, K. Zhang, H. L. Lin, X. Li, H. C. Chan, L. C.Yang, Q. S. Gao, ACS

Catal., 2017, 7, 2357-2366.

6. J. X. Feng, J. Q. Wu, Y. X. Tong, G. R. Li, J. Am. Chem. Soc., 2018, 140, 610−617.

7. X. Zhang, X. L. Yu, L. J. Zhang, F. Zhou, Y. Y. Liang, R. H. Wang, Adv. Funct. Mater., 2018, 1706523.

8. F. Z. Song, W. Li, J. Q. Yang, G. Q. Han, P. L. Liao, Y. J. Sun, Nature Commun., 2018, 9, 4531.

9. Z. Y. Chen, Y. Song, J. Y. Cai, X. S. Zheng, D. D. Han, Y. S. Wu, Y. P. Zang, S. W. Niu, Y. Liu, J. F. Zhu, X. J. Liu, G. M. Wang, Angew. Chem. Int. Ed., 2018, 57, 1-6.

10. Y. Y. Chen, Y. Zhang, X. Zhang, T. Tang, H. Luo, S. Niu, Z. H. Dai, L. J. Wan, J. S. Hu, Adv. Mater., 2017, 29, 1703311.

11. C. J. Lei, Y. Wang, Y. Hou, P. Liu, J. Yang, T. Zhang, X. D. Zhuang, M. W. Chen, B. Yang, L. C. Lei, C. Yuan, M. Qiu, X. L. Feng, Energy Environ. Sci., 2019, 12, 149-156.

12. J. S. Li, S. A. Zhang, J. Q. Sha, H. Wang, M. Z. Liu, L. X. Kong, G. D. Liu, ACS Appl. Mater. Interf., 2018, 10, 17140-17146.

13. D. W. Wang, C. Han, Z. C. Xing, Q. Li, X. R. Yang, J. Mater. Chem. A, 2018, 6, 15558-15563.

14. A. Meena, M. Ha, S. S. Chandrasekaran, S. Sultan, P. Thangavel, A. M. Harzandi, B. Singh, J. N. Tiwari, K. S. Kim, J. Mater. Chem. A, 2019, 7, 15794-15800.